Fundamental parameters of the close interacting binary HD 170582 and its luminous accretion disc

R. E. Mennickent,[1]⋆ G. Djurašević,[2] M. Cabezas,[1] A. Cséki,[2] J. G. Rosales,[1] E. Niemczura,[3] I. Araya[4] and M. Curé[4]

[1]*Departamento de Astronomía, Universidad de Concepción, Casilla 160-C, Concepción, Chile*

[2]*Astronomical Observatory, Volgina 7, 11060 Belgrade 38, Serbia*

[3]*Astronomical Institute, Wrocław University, Kopernika 11, PL-52-622 Wrocław, Poland*

[4]*Instituto de Física y Astronomía, Facultad de Ciencias, Universidad de Valparaíso, Casilla 5030, Valparaiso, Chile*

ABSTRACT

We present a spectroscopic and photometric study of the double period variable HD 170582. Based on the study of the ASAS *V*-band light curve, we determine an improved orbital period of 16.871 77 ± 0.020 84 d and a long period of 587 d. We disentangled the light curve into an orbital part, determining ephemerides and revealing orbital ellipsoidal variability with unequal maxima, and a long cycle, showing quasi-sinusoidal changes with amplitude ΔV = 0.1 mag. Assuming synchronous rotation for the cool stellar component and semidetached configuration we find a cool evolved star of $M_2 = 1.9 \pm 0.1$ M$_\odot$, $T_2 = 8000 \pm 100$ K and $R_2 = 15.6 \pm 0.2$ R$_\odot$, and an early B-type dwarf of $M_1 = 9.0 \pm 0.2$ M$_\odot$. The B-type star is surrounded by a geometrically and optically thick accretion disc of radial extension 20.8 ± 0.3 R$_\odot$ contributing about 35 per cent to the system luminosity at the *V* band. Two extended regions located at opposite sides of the disc rim, and hotter than the disc by 67 and 46 per cent, fit the light-curve asymmetries. The system is seen under inclination 67°4 ± 0°4 and it is found at a distance of 238 ± 10 pc. Specially interesting is the double line nature of He I 5875; two absorption components move in antiphase during the orbital cycle; they can be associated with the shock regions revealed by the photometry. The radial velocity of one of the He I 5875 components closely follows the donor radial velocity, suggesting that the line is formed in a wind emerging near the stream–disc interacting region.

Key words: binaries: general – stars: early-type – stars: emission-line, Be – stars: evolution – stars: mass-loss.

1 INTRODUCTION

HD 170582 (BD-14 5085, ASAS ID 183048-1447.5, α_{2000} = 18:30:47.5, δ_{2000} = −14:47:27.8, *V* = 9.66 mag, $B - V = 0.41$ mag, spectral type A9V)[1] is a poorly studied binary star catalogued eclipsing semidetached binary and with orbital period 16.8599 d in the ASAS[2] catalogue (Pojmański 1997). It is located in the region of the cool molecular cloud L 379 and was observed by Lahulla & Hilton (1992) who obtained *V* = 9.62 mag, $B - V = 0.44$ mag and $U - B = -0.27$ mag. The system is characterized by a long photometric cycle of 536 d and is the third longest period member of the Galactic double period variables

(DPVs), after V 495 Cen and V 4142 Sgr (Mennickent & Rosales 2014; Mennickent et al. 2012a). DPVs are intermediate mass interacting binaries showing a long photometric cycle lasting about 33 times the orbital period, which has been interpreted as cyclic episodes of mass-loss (Mennickent et al. 2003, 2008, 2012b; Poleski et al. 2010). More than 200 DPVs have been found in the Galaxy and the Magellanic Clouds (Mennickent 2013), but very few of them have been studied spectroscopically (e.g. Barría et al. 2013; Garrido et al. 2013). The study of HD 170852 is important to characterize DPVs in terms of their fundamental physical parameters and also to help to understand the still unknown cause for the long photometric cycle.

In this paper, we determine fundamental orbital parameters and physical parameters for the stellar components and for the accretion disc surrounding the more massive star. We use indistinctly the terms primary or gainer for the more massive star and secondary or donor for the less massive star. The analysis of the circumstellar

matter, long cycle and evolutionary stage are postponed for a forthcoming paper. In Section 2, we present the analysis of the ASAS light curve and derive photometric ephemerides. In Section 3, we present our high-resolution spectroscopy which is analysed in Section 4 determining basic parameters for the cool stellar component and the system mass ratio. In Section 5, we model the light curve with a special code including light contributions of both stars and the accretion disc, determining stellar temperatures, radii, luminosities, surface gravities and masses and the system inclination. The characteristics of the accretion disc are determined in Section 5. The spectral energy distribution (SED) is analysed in Section 6, determining reddening and distance. We end in Section 7 summarizing the main results of our research.

2 PHOTOMETRIC EPHEMERIDES

We re-analysed the ASAS light curve considering only those better quality data points labelled as A-type and B-type and rejecting outliers and a cloud of deviating points around HJD 2452471. The analysis was made on the remaining 455 data points. The period searching algorithm PDM (Stellingwerf [1978]) was used on the data set, revealing an orbital period $P_o = 16.871\,77 \pm 0.020\,84$ (the error corresponds to the half width at half-minimum of the periodogram's peak) and epoch of maximum HJD $= 2452118.2751 \pm 0.337$ d. A second periodicity was detected, $P_1 = 587$ d, with a broad asymmetrical periodogram's peak, characterized by a full width at half-minimum of 85 d and epoch for maximum HJD 2452070.88 ± 17.61 d. We noticed that the ASAS period (16.8599 d) does not fit the periodogram minimum as well as our period, probably because of the automatic character of the period searching algorithm used in this catalogue and the lack of filtering of bad data points. The light curve was disentangled with these two periods using the software written by Zbigniew Kołaczkowski and described in Mennickent et al. ([2012a]). Afterwards, the resulting disentangled light curves were folded with both periods as shown in Fig. [1], revealing an orbital modulation typical for an ellipsoidal binary but with unequal maxima and longer cycle characterized by a quasi-sinusoidal variability. The difference in maxima in the orbital light curve could indicate a non-axisymmetrical brightness distribution in the orbital plane.
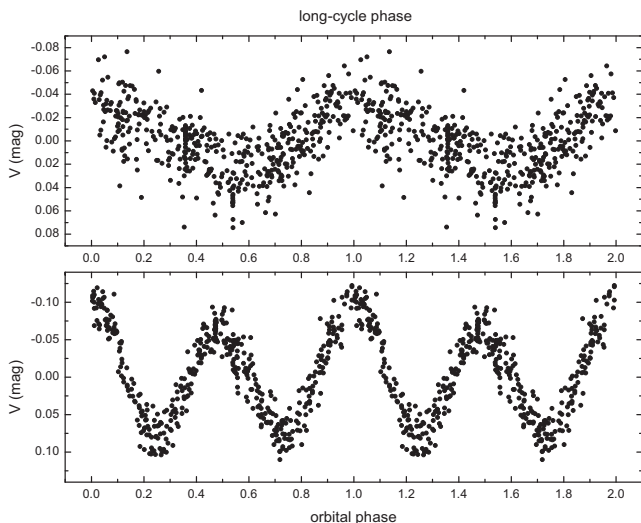

Figure 1. The disentangled ASAS light curves of HD 170582 folded with the long period (up) and the orbital period (down). Phases are calculated according to times of light-curve maxima, given by equations (1) and (2).

By phasing the disentangled light curves with their respective periods, and measuring the phases of maxima with polynomial fits, we determined the following ephemerides for the maxima of the light curves:

$$\text{HJD}_{\text{max,long}} = 2452070.9 + 587 \times E, \qquad (1)$$

$$\text{HJD}_{\text{max,orbital}} = 2452118.275(34) + 16.871(21) \times E. \qquad (2)$$

These are used for the spectroscopic analysis and discussed with the new spectroscopic ephemerides determined in Section 4.

3 SPECTROSCOPIC OBSERVATIONS

We conducted spectroscopic observations of HD 170582 since year 2008–2013 obtaining 13 optical spectra with resolution $R \sim 40\,000$ with the spectrograph CORALIE (La Silla ESO Observatory), 112 spectra with CHIRON spectrograph with $R \sim 30\,000$ (fibre mode, Cerro Tololo Inter-American Observatory, CTIO) and 11 spectra with the DuPont-echelle spectrograph with $R \sim 40\,000$ (Las Campanas Observatory, LCO).[3] The spectral regions covered were 3865–6900 Å (CORALIE), 4580–8760 Å (CHIRON) and 3600–9850 Å (DuPont-echelle).

All spectra discussed in this paper are normalized to the continuum and the radial velocities (RVs) are heliocentric ones. Reductions were done with IRAF[4] following usual procedures for echelle spectrography, including flat and bias correction, wavelength calibration and order merging.

As a measure of internal error of the wavelength calibration, we measured the position of the interstellar Na D1 line with rms accuracy of $0.5\,\text{km s}^{-1}$.

The spectra obtained with the optical fibre spectrographs CORALIE and CHIRON are not sky-subtracted. This limitation has no effect for RV and line strength measurements, since HD 170582 is bright even at full moon and we do not flux-calibrate our spectra. Details for our observational runs are given in Table [1].

4 SPECTROSCOPIC ANALYSIS

4.1 Determination of donor physical parameters

The first inspection of the spectroscopic material reveals an SB2 type binary consisting of a late-A star with sharp metallic lines and a less luminous B star with broader helium absorption lines. In addition, emission in Balmer lines is observed at some epochs suggesting that the system is an interacting binary. By comparison of relative strengths of metallic lines in the region 4500–4600 Å, devoid of lines of the hotter component, with some spectra from the UVES-POP library,[5] we find a relatively good fit with the diluted spectrum of HD 90772, hence we estimate a spectral type A9 for the cooler component, in agreement with the figure given by Houk & Smith-Moore ([1988]). Comparing luminosity-sensitive features like

---

[3] Technical descriptions for these spectrographs and their cameras can be found in www.eso.org/, http://www.ctio.noao.edu/ and http://www.lco.cl/.

[4] IRAF is distributed by the National Optical Astronomy Observatories, which are operated by the Association of Universities for Research in Astronomy, Inc., under cooperative agreement with the National Science Foundation.

[5] https://www.eso.org/sci/observing/tools/uvespop.html

Table 1. Summary of spectroscopic observations. *N* is number of spectra. The HJD at mid-exposure for the first spectrum of the series is given. Φ_o and Φ_l refer to the orbital and long-cycle phase, respectively, and are calculated according to equations (1) and (7).

UT-date	Observatory/Telescope	Instrument	N	Exptime (s)	HJD	Φ_o	Φ_l
2008-05-24	ESO/EULER	CORALIE	3	1800	2454610.882519	0.995	0.327
2008-05-25	ESO/EULER	CORALIE	2	1800	2454611.903408	0.056	0.329
2008-06-13	LCO/DuPont	Echelle	2	900	2454631.794399	0.235	0.363
2009-05-13	LCO/DuPont	Echelle	1	750	2454965.917228	0.038	0.932
2008-08-22	ESO/EULER	CORALIE	1	1200	2454701.652578	0.375	0.482
2008-08-23	ESO/EULER	CORALIE	2	1200	2454702.665820	0.435	0.483
2008-08-24	ESO/EULER	CORALIE	5	1500	2454703.630014	0.492	0.485
2009-08-24	LCO/DuPont	Echelle	4	900	2454998.638369	0.977	0.988
2009-06-15	LCO/DuPont	Echelle	4	900	2455068.596925	0.124	0.107
2012-03-29	CTIO/1.5m	CHIRON	3	1200	2456016.817323	0.324	0.722
2012-04-05	CTIO/1.5m	CHIRON	3	1200	2456023.877949	0.742	0.734
2012-04-10	CTIO/1.5m	CHIRON	3	1200	2456028.833956	0.036	0.743
2012-04-30	CTIO/1.5m	CHIRON	3	1200	2456048.725777	0.215	0.777
2012-05-05	CTIO/1.5m	CHIRON	3	1200	2456053.891370	0.521	0.785
2012-05-14	CTIO/1.5m	CHIRON	3	1200	2456062.708397	0.044	0.800
2012-05-20	CTIO/1.5m	CHIRON	3	1200	2456068.848760	0.408	0.811
2012-05-31	CTIO/1.5m	CHIRON	3	1200	2456079.881457	0.062	0.830
2012-06-04	CTIO/1.5m	CHIRON	6	1200	2456083.772875	0.292	0.836
2012-06-10	CTIO/1.5m	CHIRON	3	1200	2456089.834323	0.651	0.847
2012-06-14	CTIO/1.5m	CHIRON	2	1200	2456093.762810	0.884	0.853
2012-06-26	CTIO/1.5m	CHIRON	3	1200	2456105.720519	0.593	0.874
2012-08-11	CTIO/1.5m	CHIRON	3	1200	2456151.703993	0.318	0.952
2012-08-25	CTIO/1.5m	CHIRON	1	1800	2456165.550340	0.139	0.976
2013-03-10	CTIO/1.5m	CHIRON	1	927	2456362.918475	0.837	0.312
2013-06-05	CTIO/1.5m	CHIRON	3	1200	2456449.804977	0.987	0.460
2013-06-13	CTIO/1.5m	CHIRON	2	1500	2456457.834031	0.462	0.473
2013-06-15	CTIO/1.5m	CHIRON	3	1200	2456459.854115	0.582	0.477
2013-06-17	CTIO/1.5m	CHIRON	3	1200	2456461.827297	0.699	0.480
2013-06-19	CTIO/1.5m	CHIRON	3	1200	2456463.818915	0.817	0.484
2013-06-25	CTIO/1.5m	CHIRON	3	1200	2456469.811141	0.172	0.494
2013-06-29	CTIO/1.5m	CHIRON	3	1200	2456473.683746	0.402	0.500
2013-06-30	CTIO/1.5m	CHIRON	1	241	2456474.801975	0.468	0.502
2013-07-03	CTIO/1.5m	CHIRON	3	1200	2456477.678008	0.639	0.507
2013-07-07	CTIO/1.5m	CHIRON	3	1200	2456481.694693	0.877	0.514
2013-07-11	CTIO/1.5m	CHIRON	3	1200	2456485.709283	0.115	0.521
2013-07-13	CTIO/1.5m	CHIRON	3	1200	2456487.681643	0.232	0.524
2013-07-15	CTIO/1.5m	CHIRON	3	1200	2456489.676610	0.350	0.528
2013-07-17	CTIO/1.5m	CHIRON	3	1200	2456491.688161	0.469	0.531
2013-07-23	CTIO/1.5m	CHIRON	3	1200	2456497.691100	0.825	0.541
2013-07-27	CTIO/1.5m	CHIRON	3	1200	2456501.729047	0.064	0.548
2013-08-01	CTIO/1.5m	CHIRON	3	1200	2456506.680476	0.358	0.557
2013-08-03	CTIO/1.5m	CHIRON	3	1200	2456508.675606	0.476	0.560
2013-08-05	CTIO/1.5m	CHIRON	3	1200	2456510.636133	0.592	0.563
2013-08-10	CTIO/1.5m	CHIRON	3	1200	2456515.651580	0.889	0.572
2013-08-12	CTIO/1.5m	CHIRON	3	1200	2456517.687903	0.010	0.575
2013-08-14	CTIO/1.5m	CHIRON	3	1200	2456519.695122	0.129	0.579
2013-08-16	CTIO/1.5m	CHIRON	3	1200	2456521.675552	0.246	0.582
2013-08-20	CTIO/1.5m	CHIRON	3	1200	2456525.616642	0.480	0.589

the Fe II and Ti II double blend at 4172–4178 Å, and similar blends at 4395–4400, 4417 and 4444 Å, with less sensitive luminosity lines like Ca I 4227, Fe I 4271 and Mg II 4481, we estimate a luminosity class between I and III for the cooler star.

In order to determine the physical parameters of the A-type star, we compared our observed donor spectrum with synthetic spectra constructed with the SYNTHE code which uses atmospheric models computed with the line-blanketed LTE ATLAS9 code (Kurucz 1993). The Kurucz models are constructed with the assumptions of plane-parallel geometry and hydrostatic and radiative equilibrium of the gas. ATLAS9 was ported under GNU Linux by Sbordone (2005) and

is available online.[6] The use of an LTE grid for studying an A-type supergiant atmosphere, which could be affected by NLTE effects, could introduce an underestimation of the iron group abundances by a factor of 2–3 (Przybilla et al. 2006).

The stellar line identification and the abundance analysis in the entire observed spectral range were performed on the basis of the line list from Castelli & Hubrig (2004).[7] The theoretical

[6] http://atmos.obspm.fr/
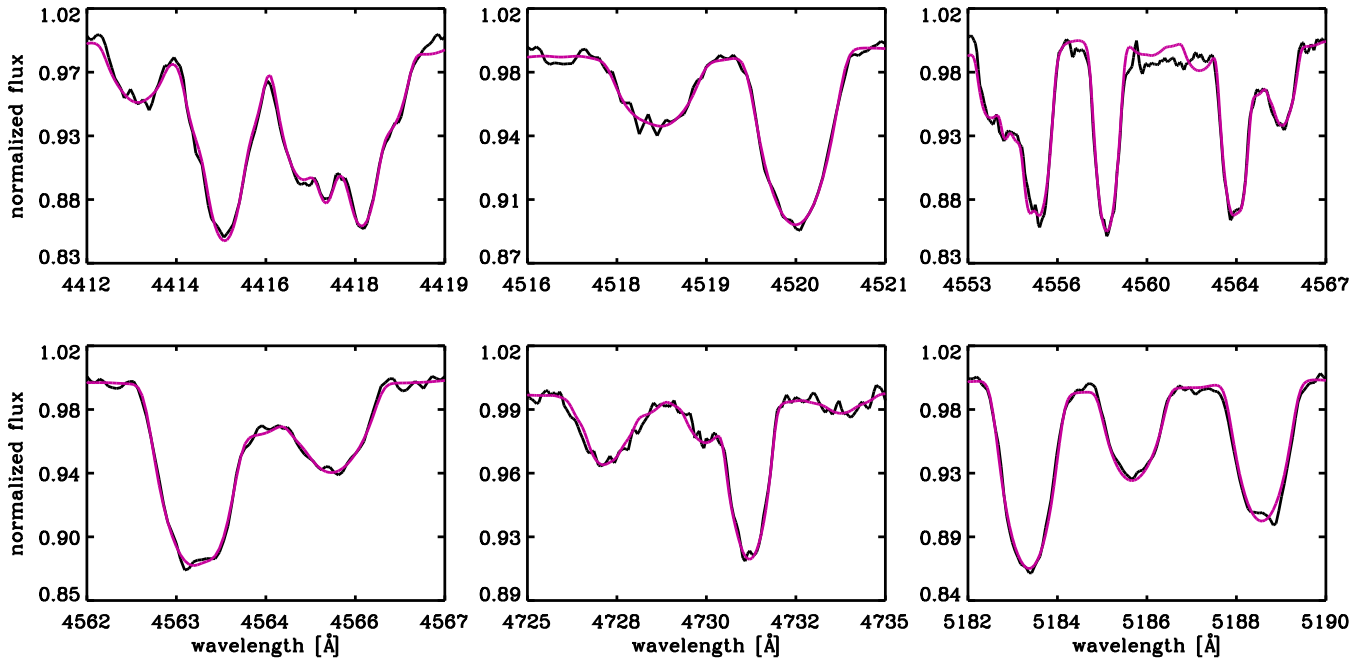[7] http://wwwuser.oat.ts.astro.it/castelli/grids.html

Figure 2. Panels showing the detailed comparison between the observed and synthetic (best model; smoothed line) donor spectrum at different spectral ranges.

models were calculated for effective temperatures from 7000 to 9000 K with steps of 100 K, surface gravities from 1.0 to 3.5 dex with the step of 0.5 dex, solar metallicity and microturbulences from 0.5 to 3.0 with the step of $0.1 \, \mathrm{km \, s^{-1}}$. As a template we choose the average donor spectrum obtained after shifting all spectra to the donor system of rest, hence removing at first order the gainer contribution. The velocities used are derived in the next section.

Our analysis follows the methodology presented in Niemczura & Połubek (2006) and relies on an efficient spectral synthesis based on a least-squares optimization algorithm. This method allows for the simultaneous determination of various parameters involved with stellar spectra and consists of the minimization of the deviation between the theoretical flux distribution and the observed normalized one. The synthetic spectrum depends on the stellar parameters, such as effective temperature T_{eff}, surface gravity $\log g$, microturbulence ξ, rotational velocity $v \sin i$, RV v_r, and the relative abundances of the elements $\varepsilon_{\mathrm{El}}$, where El denotes the individual element. The first three parameters were determined before the determination of abundances of chemical elements. The $v \sin i$ value was determined by comparing the shapes of metal line profiles with the computed profiles, as shown in Gray (2005).

The effective temperature, surface gravity and microturbulence were determined by the analysis of neutral and ionized Fe lines. In this method, we adjust T_{eff}, $\log g$ and ξ by the comparison of the abundances determined from Fe I and Fe II lines. The analysis is based on iron lines because they are the most numerous in the spectrum. In general, we require that the abundances measured from Fe I and Fe II lines yield the same result. The strength of absorption lines of Fe I depend on T_{eff}, ξ and overall metallicity Z, and are practically independent from $\log g$. On the other hand the lines of Fe II are slightly sensitive to the temperature, metallicity and most of all to gravity. First, we adjust the microturbulence until we see no correlation between iron abundances and line intensity for the Fe I lines. Secondly, T_{eff} is changed until we see no trend in the abundance versus excitation potential (EP) of the atomic level

causing the Fe I lines. Then, the gravity is obtained by fitting the Fe II and Fe I lines and by requiring the same abundances from both neutral and ionized lines.

The Fe I abundances were calculated for a series of lines characterized by different EP and line depth, in a grid of spectra spanning a range of values of $\log g$, T_{eff} and ξ. From a careful examination of these calculations, we estimated the mentioned parameters and their uncertainties.

From the above analysis, we obtained the best model characterized by $T_2 = 8000 \pm 100 \, \mathrm{K}$, $\log g_2 = 1.7 \pm 0.5$, $v_{2r} \sin i = 44 \pm 2 \, \mathrm{km \, s^{-1}}$ and $\xi = 1.0 \pm 0.7 \, \mathrm{km \, s^{-1}}$. An example of the fit of this model with the observed spectrum is shown in Fig. 2.

For these parameters, we obtained the abundances of chemical elements. We adopt the usual astronomical scale for logarithmic abundances where hydrogen is defined to be $\log \epsilon_H = 12.00$, i.e. $\log \epsilon_{\mathrm{El}} = \log (N_{\mathrm{El}}/N_H) + 12$, where N_{El} and N_H are the number densities of element El and hydrogen, respectively (Table 2). They are average abundances, which means that for example for iron it is the average abundance obtained from Fe I and Fe II lines. The Fe I abundance is equal 7.47 ± 0.16 (Fig. 3). In this figure, we show a histogram for the abundance obtained with different lines, the abundance versus line EP and the abundance versus line strength, measured as the line depth. We used line depth instead equivalent width (EW) in order to include in the analysis some weakly blended lines. The use of the line depth is justified since in general, line depth and EW should be correlated to first order and since as the resolving power through the whole spectral range is practically constant ($R \approx 30\,000$), we should expect, for a given EW, and increase of line width of 30 per cent between 4000 and 5000 Å. This means a decrease of line depth by the same order of magnitude, which should be translated into small horizontal shifts of the points in the right graph of Fig. 3, without affecting the general pattern. This will not happen if the line is saturated. If the line is on the flat or damping portion of the curve-of-growth, the assumption will fail. According to the obtained Fe abundance the metallicity of the star is approximately solar (Table 2 and Fig. 4).

Table 2. Average chemical abundances for the donor star. The standard deviation is given as the error when N, the number of parts/lines from which these abundances were derived, is larger than 2. For all the other cases ($N \leq 2$), the average error of all elements (0.23) is considered. The solar abundances are from Asplund et al. (2009).

Element (Z)	N	$\log \epsilon_{(El)}$ HD 170582	$\log \epsilon_{(El)}$ Sun
6	3	8.68 ± 0.41	8.43
8	4	8.25 ± 0.15	8.69
11	5	7.05 ± 0.09	6.24
12	7	7.46 ± 0.23	7.60
13	2	6.48 ± 0.23	6.45
14	16	7.82 ± 0.23	7.51
16	3	7.59 ± 0.37	7.12
20	17	6.34 ± 0.23	6.34
21	11	2.87 ± 0.16	3.15
22	46	4.87 ± 0.18	4.95
23	11	4.02 ± 0.26	3.93
24	43	5.67 ± 0.16	5.64
25	13	5.60 ± 0.20	5.43
26	111	7.43 ± 0.12	7.50
27	3	5.70 ± 0.08	4.99
28	22	6.32 ± 0.19	6.22
29	2	4.22 ± 0.23	4.19
30	2	4.22 ± 0.23	4.56
39	7	2.14 ± 0.19	2.21
40	7	2.58 ± 0.22	2.58
56	3	1.82 ± 0.13	2.18
60	2	1.48 ± 0.23	1.42
63	1	0.92 ± 0.23	0.52

In some Algols, the donor has transferred important part of its atmosphere into the gainer, exposing its inner layers rich in elements produced by thermonuclear fusion during the star's main-sequence evolution. In these cases, abundance analysis of the donor surface layers should reveal an excess of nitrogen and a carbon depletion (e.g. Kolbas et al. 2014, and reference therein). Our analysis shows carbon with solar abundance but with a large error, based only on three lines.

On the other hand, we find oxygen and barium underabundant and sodium and cobalt overabundant. While the case of Ba might be affected by the absence of hyperfine structure in the analysis; the interpretation of the other discrepancies is at present unclear.

4.2 RVs for the donor

RVs for the donor were measured by cross-correlating the observed spectra with a reference spectrum and then applying the velocity shift corresponding to the template velocity. This last was obtained by fitting simple Gaussians to some metallic lines, finding the central wavelength and comparing these wavelengths with the corresponding laboratory wavelengths. The cross-correlation was performed in two regions deployed of H I and He I lines, viz. 4500–4800 Å and 5050–5680 Å. The RVs are given in Table 3. Subsequent inspection revealed much larger scatter in the RVs of spectra taken at LCO and ESO, they were not considered in the following analysis, i.e. we give more confidence to CHIRON based velocities and they are used in the rest of the paper.

The RVs can be fitted with a sinusoid with RV half-amplitude $K_2 = 139.8 \pm 0.2 \, \mathrm{km \, s^{-1}}$ and zero-point $\gamma = -1.3 \pm 0.2 \, \mathrm{km \, s^{-1}}$.

A careful inspection of residuals shows a non-random distribution for the circular fit.

In order to resolve the question about the possible ellipticity of the orbit, we used the genetic algorithm PIKAIA developed by Charbonneau (1995) to find the orbital elements for HD 170582. The method consists in finding the set of orbital parameters that produces a series of theoretical velocities that minimize the function χ^2 defined as

$$\chi^2(P_o, \tau, \omega, e, K_2, \gamma)$$
$$= \frac{1}{N-6} \sum_{j=1}^{N} \left(\frac{V_j - V(t_j, P_o, \tau, \omega, e, K_2, \gamma)}{\sigma_j} \right), \quad (3)$$

where N is the number of observations, P_o is the orbital period, ω the periastron longitude, τ the time of passage per the periastron, e the orbital eccentricity, K_2 the half-amplitude of the RV for the donor and γ the velocity of the system centre of mass. V_j and V are the observed and theoretical RVs at t_j. The theoretical velocity is given by

$$V(t) = \gamma + K_2(\cos(\omega + \theta(t)) + e \cos(\omega)), \quad (4)$$

where θ is the true anomaly obtained solving the following two equations involving the eccentric anomaly E:

$$\tan\left(\frac{\theta}{2}\right) = \sqrt{\frac{1+e}{1-e}} \tan\left(\frac{E}{2}\right), \quad (5)$$

$$E - e \sin(E) = \frac{2\pi}{P_o}(t - \tau). \quad (6)$$

A range of physically reasonable parameters need to be considered so that the method converge. For the period, we used the range 10–20 d, the eccentricity was set between 0 and 1, ω between 0 and 2π, τ between the minimum julian day and this value plus P_o, K_2 between 0 and $(V_{max} - V_{min})$ and γ between V_{min} and V_{max}.

The most reliable way to get error estimates for this genetic algorithm is by Monte Carlo simulations, specifically by perturbing the best-fitting solution and computing the χ^2 of these perturbed solutions. To find the standard deviation region (σ) encompassed by the joint variation of two parameters with all other parameters at their optimized values, we draw the contour corresponding to that value of $\Delta\chi^2$ for 2 degrees of freedom that includes 68.3 per cent of the probability. In our case this corresponds to $\Delta\chi^2 = 2.30$ (Bevington & Robinson 1992, p. 212).

The best orbital elements along with their estimated errors are given in Table 4. The RVs and the best fit are shown in Fig. 5, along with the re-phased disentangled orbital light curve. We notice that the RV and the light curve match the expectation for a close binary seen under an intermediate inclination, where the distorted stellar atmospheres show maximum projected surface (and brightness) just at times of RV extremes. We find that the elliptical solution provides a much better fit than the circular case, since it gives residuals without systematic trends and also a smaller χ^2 value, viz. 2.39 versus 8.38. We note that our eccentric solution gives a small e value (0.01) but it is highly significant, according to the statistical test 'p_1' of Lucy (2005). In fact, following Lucy's definition, we calculated $p_1 = 2.5 \times 10^{-29}$ satisfying the condition less than 0.05 for a significant ellipticity.

Using the results above, we calculated the time for the inferior conjunction of the donor finding the following ephemerides:

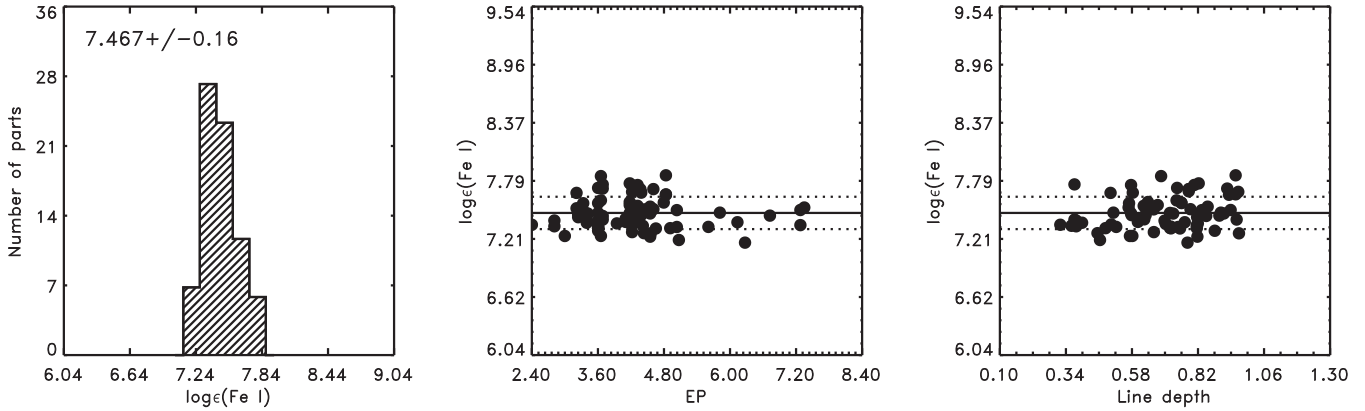$$\mathrm{HJD}_0 = (2456028.226 \pm 0.014) + (16.8722 \pm 0.0017) \times E. \quad (7)$$

Figure 3. Example of our calculations of Fe I abundance for $\log g = 1.7$, $\xi = 1.0$ and $T_{\text{eff}} = 8000$ K for lines of different EP and depth. Left-hand panel shows the average value and standard deviation.
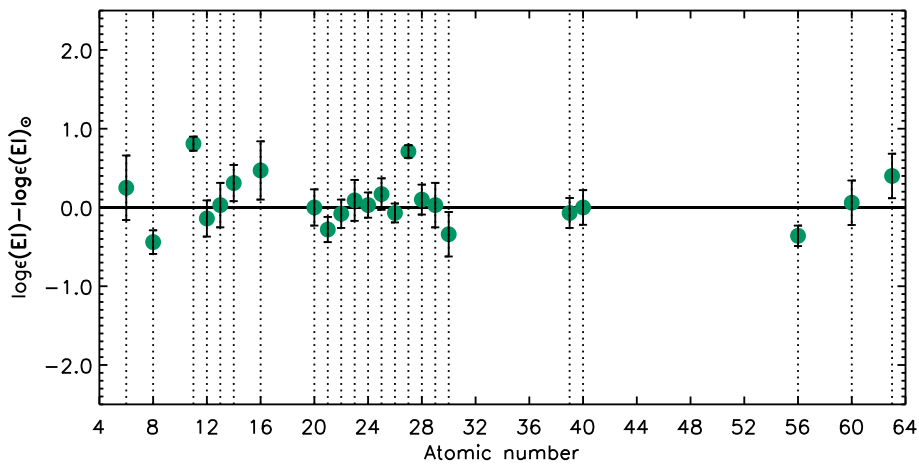

Figure 4. Comparison between the abundances obtained from different elements and the solar values from Asplund et al. (2009).

This ephemerides is used for orbital phases in the rest of the paper whereas the phases for the long cycle refer to the ephemerides given by equation (1).

It has been pointed out that gas stream and circumstellar matter can distort spectroscopic features in semidetached interacting binaries, producing skewed RVs and artificial small eccentricities (e.g. Lucy 2005). For a non-interacting binary with the stellar and orbital parameters of HD 170582, dynamical tides should have circularized the orbit and synchronized the rotational periods (Zahn 1975, 1977). This should imply that the observed small eccentricity can be spurious. However, as we will show later, the system is found with a circumprimary disc produced by mass transferred from the donor. It is possible, but not here demonstrated, that the observed eccentricity could be the result of dynamical perturbations introduced by the accretion disc. If critical velocity is rapidly reached, as suggested by Packet (1981) and de Mink, Pols & Glebbeek (2007), then the disc could turn to be relatively massive, due to the inadequacy of the gainer of accreting more material. This last point has been debated; Petrovic, Langer & van der Hucht (2005) assume that accretion ceases when the mass gaining star reaches Keplerian rotation. On the contrary, Popham & Narayan (1991) argue that a star near critical rotation can sustain accretion due to viscous coupling between the star and the disc. In the case of HD 170582, considering the luminous bright spots reported in Section 5, the disc could be relatively massive with asymmetrical mass distribution and hence to produce a small but non-zero orbital eccentricity.

4.3 Gainer, mass ratio and circumstellar matter

A gainer of B-type is suggested by the detection of H I and He I absorption lines. Mg II is dominated by the donor while the contribution of the gainer to this line is weak, if present; this indicates an early B-type for the gainer. The helium lines are contaminated by emission and show variable line profile shape, especially during high state. They are rather broad therefore the gainer might be a rapidly rotating dwarf. The Hα line is sometimes a sharp absorption with two cores, and the difference with the donor spectrum reveals a prominent double emission with deep central absorption (Fig. 6). This finding supports the interacting binary nature for this system and suggests it is in a semidetached stage. He I 5875 is very interesting since it shows two components moving in opposite directions (Fig. 7). During low stage (Φ_l between 0.2 and 0.8) the RV of the main He I 5875 component C1 (after deblending by its nearby component) as well as the He I 7065 line, can be fitted with a sine function of amplitude 75.1 ± 2.7 km s^{-1} and zero-point 20.6 ± 2.3 km s^{-1} (Fig. 8). The secondary component C2 can be fitted with a sine of amplitude 127.2 ± 1.8 km s^{-1} and zero-point 11.8 ± 1.4 km s^{-1}. This curve lags the donor RV curve only by $\Delta\Phi = 0.004 \pm 0.003$, i.e. it practically follows the donor motion. However, around $\Phi_o = 0.75$, the velocities turn to be less negative, which does not occurs around the other quadrature at $\Phi_o = 0.25$ (Fig. 8). These velocities are given in Table 5 and parameters for the RV fits are given in Table 6.

Table 3. RVs of the donor and their errors.

HJD	RV (km s^{-1})	Error (km s^{-1})	HJD	RV (km s^{-1})	Error (km s^{-1})
2456016.817323	123.077	0.576	2456463.846797	−129.481	0.553
2456016.831268	122.705	0.561	2456469.811141	124.138	0.466
2456016.845214	122.151	0.563	2456469.825082	124.197	0.484
2456023.877949	−138.305	0.918	2456469.839868	124.374	0.471
2456023.891893	−138.747	1.076	2456473.683746	78.948	0.483
2456023.905839	−139.238	0.881	2456473.697687	78.744	0.551
2456028.833956	31.288	0.777	2456473.711628	78.730	0.528
2456028.847900	31.417	0.690	2456474.801975	24.714	0.667
2456028.861845	32.741	0.777	2456477.678008	−105.880	0.477
2456048.725777	137.003	0.934	2456477.691950	−106.418	0.481
2456048.739722	136.574	0.927	2456477.705890	−106.300	0.454
2456048.753667	135.962	1.421	2456481.694693	−101.678	0.421
2456053.891370	−19.690	0.872	2456481.708634	−100.842	0.457
2456053.905316	−24.102	1.593	2456481.722574	−99.809	0.394
2456053.919262	−21.101	0.690	2456485.709283	92.776	0.564
2456062.708397	37.087	0.694	2456485.723224	93.303	0.526
2456062.722342	39.364	0.791	2456485.737165	94.899	0.624
2456062.736286	38.642	0.459	2456487.681643	139.918	0.478
2456068.848760	75.111	0.486	2456487.695584	140.020	0.501
2456068.862704	74.932	0.677	2456487.709524	140.105	0.460
2456068.876649	73.976	0.542	2456489.676610	111.141	0.525
2456079.881457	51.508	0.463	2456489.690549	110.660	0.510
2456079.895401	53.076	0.439	2456489.704490	110.331	0.516
2456079.909346	52.806	0.443	2456491.688161	24.047	0.436
2456083.772875	132.789	0.567	2456491.702101	23.108	0.554
2456083.786819	131.921	0.498	2456491.716043	23.022	0.525
2456083.800763	132.396	0.561	2456497.691100	−127.555	0.510
2456083.815193	132.305	0.597	2456497.705041	−127.102	0.516
2456083.829138	131.286	0.559	2456497.718983	−126.540	0.497
2456083.843082	132.661	0.679	2456501.729047	54.682	0.550
2456089.834323	−111.254	0.838	2456501.742986	55.338	0.561
2456089.834323	−111.254	0.842	2456501.756926	55.363	0.432
2456089.834323	−111.254	0.847	2456506.680476	106.396	0.603
2456093.762810	−96.119	0.490	2456506.694416	106.082	0.546
2456093.776754	−95.180	0.733	2456506.708355	105.110	0.566
2456105.720519	−77.838	0.442	2456508.675606	17.626	0.641
2456105.734460	−78.346	0.478	2456508.689546	18.238	0.872
2456105.748401	−79.092	0.464	2456508.703486	16.241	1.755
2456151.703993	125.185	0.575	2456510.636133	−76.643	0.494
2456151.717933	125.114	0.657	2456510.650074	−77.083	0.487
2456151.731873	124.450	0.692	2456510.664855	−78.440	0.517
2456165.550340	107.411	0.503	2456515.651580	−93.099	0.426
2456449.804977	−13.799	0.500	2456515.665520	−91.941	0.439
2456449.818917	−12.957	0.276	2456515.686404	−91.941	0.440
2456449.832859	−12.406	0.343	2456517.687903	5.802	0.468
2456457.834031	29.909	0.484	2456517.701843	5.918	0.465
2456457.851445	28.075	0.643	2456517.715784	7.180	0.627
2456459.854115	−70.808	0.447	2456519.695122	101.865	0.443
2456459.868057	−71.100	0.392	2456519.709062	102.380	0.495
2456459.881998	−72.264	0.640	2456519.723001	102.046	0.490
2456461.827297	−131.490	0.622	2456521.675552	139.573	0.481
2456461.841237	−133.005	0.577	2456521.689492	139.634	0.510
2456461.855179	−132.800	0.528	2456521.703432	139.566	0.488
2456463.818915	−130.404	0.517	2456525.616642	15.008	0.572
2456463.832856	−129.967	0.493	2456525.630581	13.725	0.612
2456525.644520	12.044	0.568			

If we use the system inclination $i = 67°$ derived in Section 5, and the basic kinematics formula:

$$\frac{r}{R_\odot} = \frac{Pv}{50.633},$$ (8)

where r represents the radial distance from the centre of rotation, P the rotational period in days and v the linear orbital velocity of material moving in the orbital plane measured in km s^{-1}, then we can find the position of the light-centres of the line components listed in Table 6. We find for C1 a light centre located $r = 27.1$ R$_\odot$ from the centre of mass pointing 216° from the line joining the stellar centres

Table 4. Orbital elements for the donor of HD 170582 obtained by minimization of the χ^2 parameter given by equation (1). The value $\tau^* = \tau - 2450\,000$ is given and also the maximum and minimum quantity in one isophote 1σ.

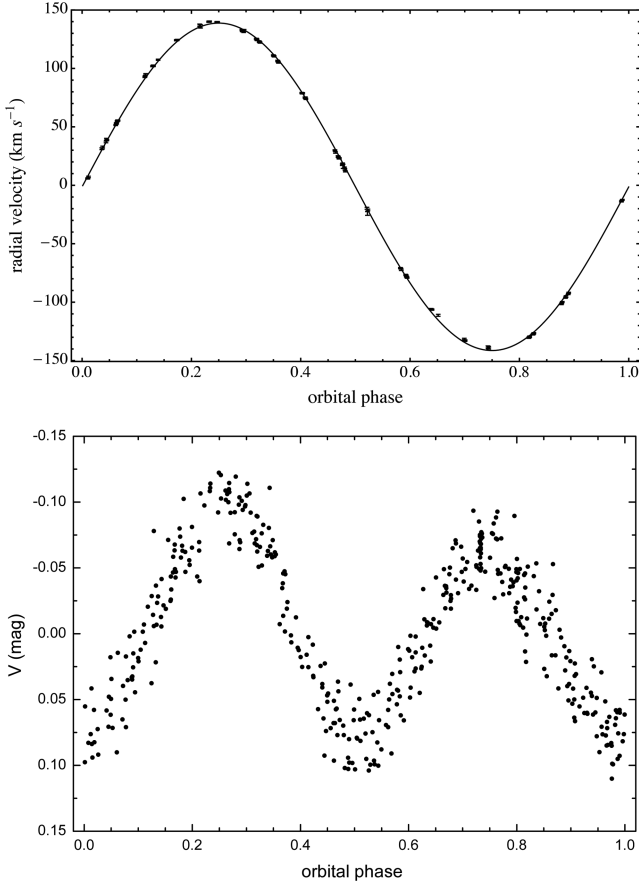| Parameter	Best value	Lower limit	Upper limit
P_o (d)	16.8722	16.8705	16.8739
τ^*	6029.56	6027.90	6030.96
e	0.0133	0.0055	0.0205
ω (red)	5.208	5.183	5.231
K_2 (km s^{-1})	140.1	139.0	141.2
γ (km s^{-1})	−1.30	−2.05	−0.55

Figure 5. Upper panel: the donor RVs and the best fit, given by equation (4) and the parameters of Table 4. The RV error bars are also shown, but they are usually smaller than the used symbols. Lower panel: disentangled orbital light curve. In both panels phases are calculated according to times of donor inferior conjunction, given by equation (7).

measured in the direction opposite to the orbital motion. For C2, we find the light centre located at $r = 45.9\,\mathrm{R}_\odot$ from the centre of mass, pointing 1°4 from the line joining the stellar centres, as measured in the direction opposite to the orbital motion. The meaning of these positions will be discussed in Section 5.2.

From the above and also considering the irregular line profiles, it seems that the helium lines are not fully formed in the gainer stellar photosphere, but they can be partly formed in the circumstellar material. Actually, the overall helium lines cannot be fitted by conventional synthetic line profiles of photospheric models; the line width changes and the depth is usually larger than expected for an
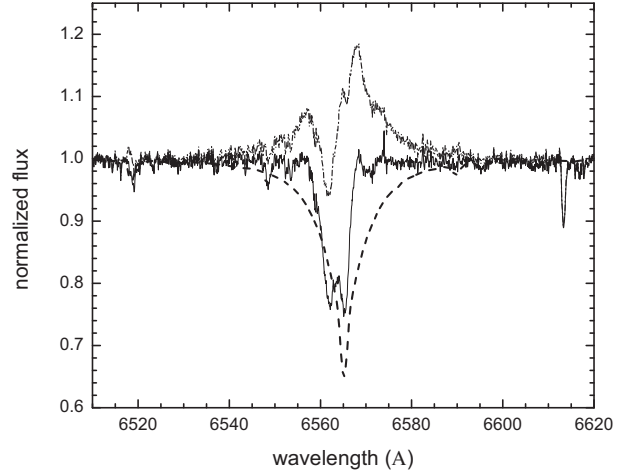

Figure 6. Hα line on HJD 2456506.680476 ($\Phi_o = 0.36$, $\Phi_1 = 0.56$) over-plotted with the donor synthetic spectrum (thick dashed line) and the difference spectrum vertically shifted by $+1$.
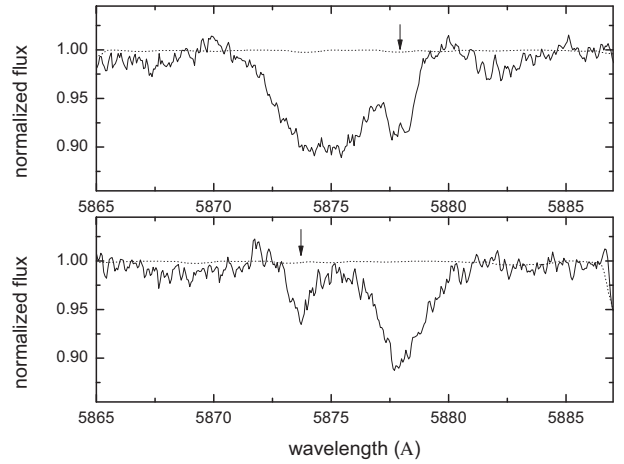

Figure 7. He I 5875 lines for HJD 2456489.690549 ($\Phi_o = 0.35$, $\Phi_1 = 0.53$, up) and HJD 2456497.705041 ($\Phi_o = 0.83$, $\Phi_1 = 0.54$, down). The synthetic donor at the right velocity system is indicated with dotted lines and the arrow indicates the second He I 5875 component.
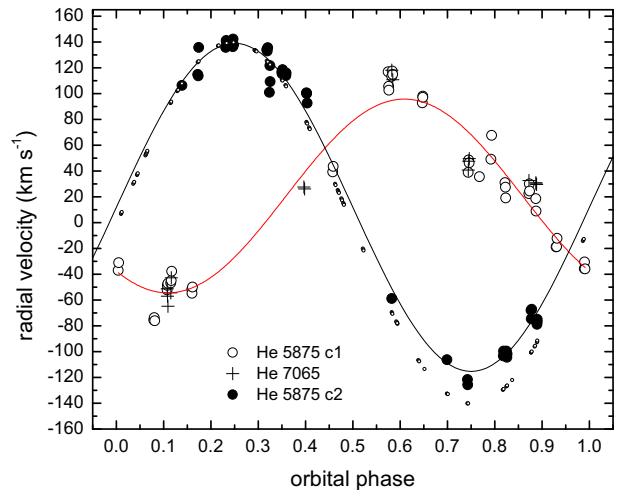

Figure 8. RV for the He 5875 (components c1 and c2) and He 7065 lines and the best sine fits. Small circles show the donor RV at the observation epochs.

Table 5. RVs of helium lines with typical error $3\,\mathrm{km\,s^{-1}}$.

HJD	Φ_o	Φ_1	RV$_{5875}$ C1 (km s^{-1})	RV$_{5875}$ C2 (km s^{-1})	RV$_{7065}$ (km s^{-1})
2456016.817323	0.324	0.722	−75.5	100.9	–
2456016.831268	0.325	0.722	−73.7	121.7	–
2456016.845214	0.325	0.722	−76.2	109.3	–
2456023.877949	0.742	0.734	–	−121.7	–
2456023.891893	0.743	0.734	–	−125.8	–
2456028.833956	0.036	0.743	49.0	–	–
2456028.861845	0.038	0.743	67.6	–	–
2456151.703993	0.318	0.952	–	134.0	–
2456151.717933	0.319	0.952	–	133.0	–
2456151.731873	0.320	0.952	–	135.6	–
2456165.550340	0.139	0.976	–	106.4	–
2456449.804977	0.987	0.460	38.8	–	40.7
2456449.818917	0.987	0.460	48.6	–	47.6
2456449.832859	0.988	0.460	46.3	–	49.6
2456459.854115	0.582	0.477	–	−58.8	–
2456461.827297	0.699	0.480	–	−106.3	–
2456461.841237	0.700	0.480	39.2	–	–
2456461.855179	0.701	0.480	43.5	–	–
2456463.818915	0.817	0.484	116.8	–	–
2456463.832856	0.818	0.484	105.6	−103.4	–
2456463.846797	0.819	0.484	102.6	−99.7	–
2456469.811141	0.172	0.494	−18.9	114.8	–
2456469.825082	0.173	0.494	−18.7	113.7	–
2456469.839868	0.174	0.494	−12.3	135.7	–
2456473.683746	0.402	0.500	−51.9	100.5	–
2456473.697687	0.403	0.501	−54.8	100.0	–
2456473.711628	0.404	0.501	−50.0	92.6	–
2456477.678008	0.639	0.507	–	–	27.6
2456477.705890	0.640	0.507	–	–	26.2
2456481.694693	0.877	0.514	–	−67.9	–
2456481.708634	0.878	0.514	–	−74.7	–
2456481.722574	0.878	0.514	–	−67.2	–
2456485.709283	0.115	0.521	22.4	–	32.6
2456485.723224	0.115	0.521	30.0	–	–
2456485.737165	0.116	0.521	24.5	–	–
2456487.681643	0.232	0.524	−35.8	135.8	–
2456487.695584	0.232	0.524	−30.5	141.1	–
2456487.709524	0.233	0.524	−36.0	138.4	–
2456489.676610	0.350	0.528	−52.3	116.8	−51.3
2456489.690549	0.351	0.528	−48.7	115.4	−57.1
2456489.704490	0.351	0.528	−47.3	118.6	−64.8
2456497.691100	0.825	0.541	113.3	−99.6	118.1
2456497.705041	0.826	0.541	117.4	−104.5	–
2456497.718983	0.826	0.541	114.9	−101.8	110.8
2456501.729047	0.064	0.548	31.0	–	–
2456501.742986	0.065	0.548	27.5	–	–
2456501.756926	0.066	0.548	19.1	–	–
2456506.680476	0.358	0.557	−46.8	116.0	−54.4
2456506.694416	0.358	0.557	−45.0	113.9	−42.8
2456506.708355	0.359	0.557	−37.8	115.9	–
2456515.651580	0.889	0.572	92.8	−78.9	–
2456515.665520	0.890	0.572	97.9	−76.8	–
2456515.686404	0.649	0.572	97.1	−75.0	–
2456517.687903	0.010	0.575	35.6	–	–
2456519.695122	0.129	0.579	18.5	–	30.9
2456519.709062	0.130	0.579	8.8	–	30.0
2456519.723001	0.131	0.579	–	–	29.6
2456521.675552	0.246	0.582	−37.0	136.2	–
2456521.689492	0.247	0.582	−31.1	142.3	–
2456521.703432	0.248	0.582	–	137.7	–
2456525.616642	0.480	0.589	–	137.7	–

Table 6. Results of the sinusoidal fits ($\gamma + K \sin(2\pi(\Phi_o - \delta))$) to the RV curves of the He I 5875 components. The root-mean-square of the fits are also given. The parameters γ, K and rms are given in km s^{-1}.

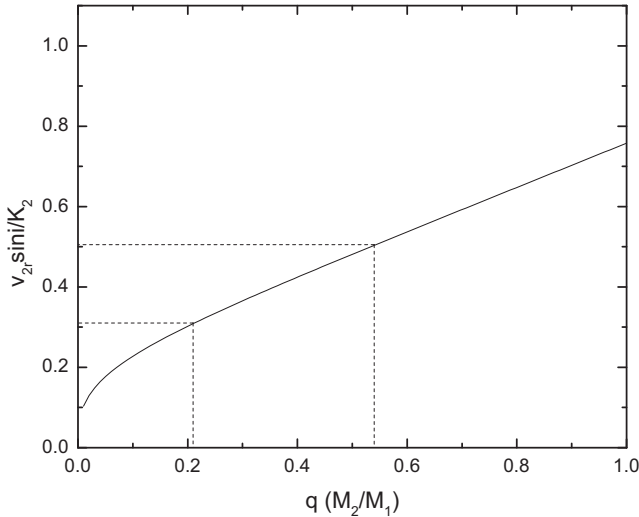| Line	γ	K	δ	rms
He I 5875 C1	20.6 ± 2.3	75.1 ± 2.7	0.601 ± 0.008	15.3
He I 5875 C2	11.8 ± 1.4	127.2 ± 1.8	0.004 ± 0.003	7.9

Figure 9. Relative donor rotational velocity versus mass ratio ($q = M_2/M_1$). The solid line is given by equation (9) and the dashed lines show the synchronous ($q = 0.21$) and the observed (subsynchronous, $q = 0.54$) cases.

early B-type gainer contributing about 50 per cent to the total light. This number comes from the veiling factor applied to the donor synthetic spectrum to match the observed metallic lines in Section 4.1. We considered the possibility that both components are artefacts produced by the motion of a central emission feature; however, in this case we should observe both absorption components moving in phase which is not observed.

Let us assume for now that the helium velocities of component C1 represent the gainer orbital motion, then the inferred mass ratio is $q = 0.54 \pm 0.01$. We can investigate if this value is compatible with synchronous rotation for the secondary star. For a secondary star filling its Roche lobe in corotation with the binary:

$$\frac{v_{2r}\sin i}{K_2} \approx (1 + q)\frac{0.49q^{2/3}}{0.6q^{2/3} + \ln(1 + q^{1/3})} \quad (9)$$

(Eggleton 2006, equation 3.9). Using the above equation, $K_2 = 140.1$ km s^{-1} and $v_{2r} \sin i = 44$ km s^{-1}, we obtain $q \approx 0.21$, much lower than the q value derived from helium lines (Fig. 9). This indicates that the donor is rotating subsynchronously or that the helium lines do not represent the motion of the gainer. We argue now against the first assumption. Synchronization time-scales for early type stars are 100–1000 times shorter than circularization time-scales (Hilditch 2001). As the system is almost circularized ($e = 0.013$, Table 4), there is no reason to suspect a non-synchronous donor. We are left with the explanation that C1 is not formed in the gainer stellar photosphere. Their origin could be an accretion disc around the gainer, with asymmetrical brightness distribution, to account for the non-equal maxima in the light curve. We find support for this hypothesis in our light-curve analysis presented in Section 5. The mass ratio $q = 0.21$ is favoured in this paper, since it is

consistent with donor spin synchronization and is also justified by arguments about stellar masses and disc formation given in the next section.

4.4 Mass constrains from spectroscopy

The system mass function for a binary in a circular orbit can be expressed as

$$f = \frac{M_2 \sin^3 i}{q(1 + q)^2} = 1.0361 \times 10^{-7} \left(\frac{K_2}{\text{km s}^{-1}}\right)^3 \frac{P_o}{\text{day}} \, M_\odot. \quad (10)$$

The f value derived from our RV study is 4.81 ± 0.01 M$_\odot$. Using $q = 0.21$ (donor rotating synchronously), we get $M_2 > 1.48$ M$_\odot$ and $M_1 > 7.05$ M$_\odot$. On the other hand, if $q = 0.54$ we derive $M_2 > 6.16$ M$_\odot$ and $M_1 > 11.41$ M$_\odot$. These masses turns to be too high for the temperatures derived from spectroscopy and this fact supports the $q = 0.21$ solution.

To check if the formation of an accretion disc is possible, we calculate the distance to closest approach, measured from the centre of the gainer, of a stream coming from the inner Lagrangian point L_1:

$$r_{\min} = 0.0488q^{-0.464}a \quad (11)$$

(Lubow & Shu 1975). For $q = 0.21$, we get $r_{\min} = 0.10\,a$. i.e. 6.1 R$_\odot$ (0.065 a or 4.0 R$_\odot$ for $q = 0.54$). When comparing with the gainer radius of 5.4 R$_\odot$ we observe that for the low mass ratio solution the disc can be formed ($r_{\min} > R_1$) but not for the high mass ratio case, when an impact system should be observed where the gas stream directly impacts the gainer.

5 LIGHT-CURVE MODEL AND SYSTEM PARAMETERS

5.1 The fitting procedure

The light-curve fitting was performed using the Nelder–Mead simplex algorithm (see e.g. Press et al. 1992) with optimizations described by Dennis & Torczon (1991), and the model of a binary system with a disc described in the previous section. For more detail see e.g. Djurašević (1992).

To obtain reliable estimates of the system parameters, a good practice is to restrict the number of free parameters by fixing some of them to values obtained from independent sources. In this section, we use subindexes 1 and 2 for labelling parameters of the hot and cool star, respectively. We fixed the mass ratio to $q = 0.21$ and the stellar temperatures to $T_1 = 18\,000$ K and $T_2 = 8000$ K based on our spectroscopic results. The hotter temperature was selected to provide a good fit to the SED as explained in Section 6. The implications of this choice are discussed at the end of Section 5.2. In addition, we set the gravity-darkening coefficient and the albedo of the gainer and the donor to $\beta_{1,2} = 0.25$ and $A_{1,2} = 1.0$ in accordance with von Zeipel's law for radiative envelopes (von Zeipel 1924) and complete re-radiation (Rafert & Twigg 1980). The limb-darkening for the components was calculated in the way described by Djurašević et al. (2010).

The possible values of free parameters are constrained by imposing the lowest and highest values which seem reasonable based on previous studies of this binary. Here, are the ranges for the fitted parameters.

(i) Inclination: $50°.0 \, 70°.0$.

(ii) Disc dimension factor (the ratio of the disc radius and the radius of the critical Roche lobe along the *y*-axis): 0.5–0.9.

(iii) Disc edge temperature: 4000–8000 K.

(iv) Disc edge thickness: 0.02–0.06 (in units of a_{orb}).

(v) Disc centre thickness: 0.13–0.17 (in units of a_{orb}).

(vi) The exponent of the disc temperature distribution: 6.0–8.0.

After the first fit, these ranges were decreased according to the results of the first iteration.

We treated the rotation of the donor as synchronous ($f_2 = 1.0$), since it is assumed that the donor has filled its Roche lobe (i.e. the filling factor of the donor was set to $F_2 = 1.0$). Although it is expected that the accreted material from the disc would transfer enough angular momentum to increase the rotation rate of the gainer to the critical velocity (Packet [1981](#); de Mink, Pols & Glebbeek [2007](#)), our study cannot discriminate between synchronous and non-synchronous gainer, probably because it is partly hidden by the accretion disc and rotationally sensitive absorption lines are produced in the disc more that in the gainer. For this reason, we present both solutions in this paper; they practically do not differ in physical parameters.

We were able to model the asymmetry of the light curve very precisely by incorporating two regions of enhanced radiation on the disc: the hotspot (hs), and the bright spot (bs). The hotspot and the bright spot in our model are located on the edge side of the disc and are described by the longitude of the centre of the spot, the angular dimension of the spot, and the temperature ratio of the spot and the unperturbed local temperature of the disc. The difference between the temperature of the spot and the local unperturbed temperature of the disc is what results in the difference in brightness. Location of the hotspot is calculated from the assumption that the gas stream from the L1 point falls tangentially on to the disc. The bright spot can be located at any longitude. The angular dimension of the spots was constrained to the range from 10° to 40° for the hotspot, and from 10° to 90° for the bright spot; the temperature ratio for the spots can be from 1.0 to 2.0. The incorporation in the model, of extended spots at the disc outer rim, follows results of hydrodynamical simulations of gas dynamics in interacting close binary stars showing similar structures (e.g. Bisikalo et al. [2003](#)), as explained in detail in the next section.

5.2 The best light-curve model

The fit, O−C residuals, individual flux contributions of the donor, disc and the gainer, and the view of the optimal model at orbital phases 0.25, 0.50 and 0.75, obtained with the parameters estimated by the light-curve analysis, are illustrated in Fig. [10](#) for the gainer's synchronous case. We note that residuals show no dependence on orbital or long-cycle phases and that the best-fitting model of HD 170582 contains an optically and geometrically thick disc around the hotter, more massive gainer star. Our results for the synchronic gainer are shown in Table [7](#) and those for a gainer rotating at critical velocity in Table [8](#). Small differences are found in the physical parameters of both cases. It is reasonable to assume that the true parameters of the system are found in between both solutions. For simplicity, we discuss here the synchronous case only.

The best model shows that the inclination angle is well constrained to 67°.4 ± 0°.4. With a radius of $R_d \approx 20.8\,R_\odot$, the disc is 3.8 times larger than the central star ($R_h \approx 5.5\,R_\odot$). The disc has a convex shape, with central thickness $d_c \approx 9.5\,R_\odot$ and edge thickness $d_e \approx 2.3\,R_\odot$. The temperature of the disc increases from $T_d = 5410\,K$ at its edge, to $T_h = 18\,000\,K$ at the inner radius,
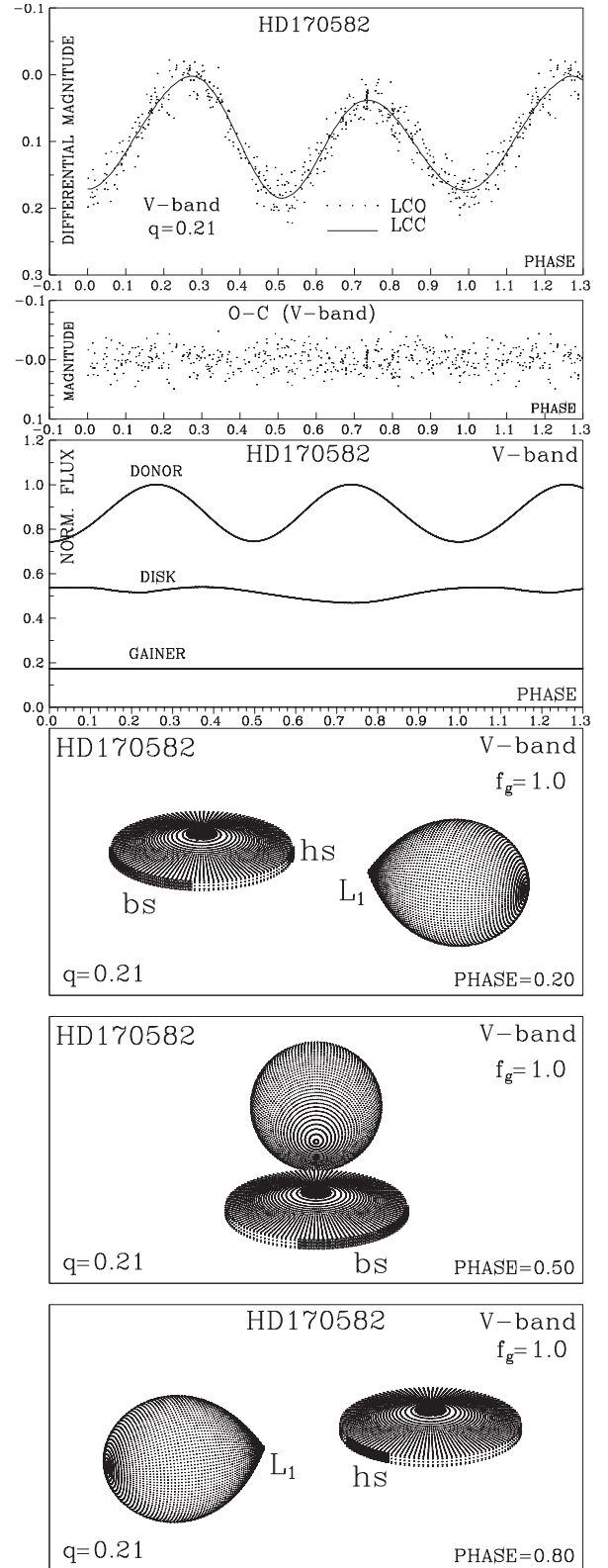

Figure 10. Observed (LCO) and synthetic (LCC) light curves of HD170582 obtained by analysing *V*-band photometric observations; final O−C residuals between the observed and optimum synthetic light curves; fluxes of donor, gainer and of the accretion disc, normalized to the donor flux at phase 0.25; the views of the optimal model at orbital phases 0.20, 0.50 and 0.80, obtained with parameters estimated by the light-curve analysis.

Table 7. Results of the analysis of HD170582 V-band light curve obtained by solving the inverse problem for the Roche model with an accretion disc around the more-massive (hotter) gainer in synchronous rotation regime.

Quantity		Quantity	
n	455	$\mathcal{M}_1 [\mathrm{M}_\odot]$	9.0 ± 0.2
$\Sigma(\mathrm{O} - \mathrm{C})^2$	0.1513	$\mathcal{M}_2 [\mathrm{M}_\odot]$	1.9 ± 0.1
σ_{rms}	0.0182	$\mathcal{R}_1 [\mathrm{R}_\odot]$	5.5 ± 0.2
$i[°]$	67.4 ± 0.4	$\mathcal{R}_2 [\mathrm{R}_\odot]$	15.6 ± 0.2
F_d	0.65 ± 0.02	$\log g_1$	3.90 ± 0.1
$T_\mathrm{d}[\mathrm{K}]$	5410 ± 200	$\log g_2$	2.33 ± 0.1
$d_\mathrm{e}[a_\mathrm{orb}]$	0.155 ± 0.004	M_bol^1	-3.9 ± 0.2
$d_2[a_\mathrm{orb}]$	0.038 ± 0.004	M_bol^2	-2.6 ± 0.1
a_T	7.3 ± 0.3	$a_\mathrm{orb}[\mathrm{R}_\odot]$	61.2 ± 0.2
f_1	1.00	$\mathcal{R}_\mathrm{d}[\mathrm{R}_\odot]$	20.8 ± 0.3
F_1	0.187 ± 0.004	$d_\mathrm{e}[\mathrm{R}_\odot]$	2.3 ± 0.1
$T_1[\mathrm{K}]$	18000	$d_\mathrm{c}[\mathrm{R}_\odot]$	9.5 ± 0.1
$T_2[\mathrm{K}]$	8000		
$A_\mathrm{hs} = T_\mathrm{hs}/T_\mathrm{d}$	1.66 ± 0.1		
$\theta_\mathrm{hs}[°]$	19.6 ± 2.0		
$\lambda_\mathrm{hs}[°]$	333.6 ± 6.0		
$\theta_\mathrm{rad}[°]$	27.0 ± 5.0		
$A_\mathrm{bs} = T_\mathrm{bs}/T_\mathrm{d}$	1.46 ± 0.1		
$\theta_\mathrm{bs}[°]$	56.2 ± 3.0		
$\lambda_\mathrm{bs}[°]$	134.8 ± 6.0		
Ω_1	11.26 ± 0.04		
Ω_2	2.26 ± 0.02		

Note: Fixed parameters: $q = \mathcal{M}_2/\mathcal{M}_1 = 0.21$ – mass ratio of the components, $T_1 = 18\,000$ K; $T_2 = 8000$ K – temperature of the more massive (hotter) gainer and less-massive (cooler) donor, respectively, $F_2 = 1.0$ – filling factor for the critical Roche lobe of the donor, $f_{1,2} = 1.00$ – nonsynchronous rotation coefficients of the system components, $\beta_{1,2} = 0.25$ – gravity-darkening coefficients of the components, $A_{1,2} = 1.0$ – albedo coefficients of the components.

Note: n – number of observations, $\Sigma(\mathrm{O} - \mathrm{C})^2$ – final sum of squares of residuals between observed (LCO) and synthetic (LCC) light curves, σ_{rms} – root-mean-square of the residuals, i – orbit inclination (in arcdegrees), $F_\mathrm{d} = R_\mathrm{d}/R_\mathrm{yc}$ – disc dimension factor (the ratio of the disc radius to the critical Roche lobe radius along y-axis), T_d – disc-edge temperature, d_e, d_c, – disc thicknesses (at the edge and at the centre of the disc, respectively) in the units of the distance between the components, a_T – disc temperature distribution coefficient, f_g – non-synchronous rotation coefficient of the more massive gainer (in the synchronous rotation regime), $F_1 = R_1/R_\mathrm{zc}$ – filling factor for the critical Roche lobe of the hotter, more-massive gainer (ratio of the stellar polar radius to the critical Roche lobe radius along z-axis for a star in synchronous rotation regime), $A_\mathrm{hs,\,bs} = T_\mathrm{hs,\,bs}/T_\mathrm{d}$ – hot and bright spots' temperature coefficients, $\theta_\mathrm{hs,\,bs}$ and $\lambda_\mathrm{hs,\,bs}$ – spots' angular dimensions and longitudes (in arcdegrees), θ_rad – angle between the line perpendicular to the local disc edge surface and the direction of the hotspot maximum radiation, $\Omega_{1,\,2}$ – dimensionless surface potentials of the hotter gainer and cooler donor, $\mathcal{M}_{1,2}[\mathrm{M}_\odot]$, $\mathcal{R}_{1,2}[\mathrm{R}_\odot]$ – stellar masses and mean radii of stars in solar units, $\log g_{1,2}$ – logarithm (base 10) of the system components effective gravity, $M_\mathrm{bol}^{1,2}$ – absolute stellar bolometric magnitudes, $a_\mathrm{orb}[\mathrm{R}_\odot]$, $\mathcal{R}_\mathrm{d}[\mathrm{R}_\odot]$, $d_\mathrm{e}[\mathrm{R}_\odot]$, $d_\mathrm{c}[\mathrm{R}_\odot]$ – orbital semimajor axis, disc radius and disc thicknesses at its edge and centre, respectively, given in solar units.

where it is in thermal and physical contact with the gainer. The relatively large disc temperature gradient explains the big difference between disc thickness at the inner and outer edges. In our model, the gainer rotates synchronously with lineal velocity $v_{1\mathrm{r}} = v_{2\mathrm{r}}(R_1/R_2) = 15.5\,\mathrm{km\,s^{-1}}$. The surface gravity for the giant is larger than the figure obtained from the spectroscopic analysis ($\log g = 2.3 \pm 0.1$ versus $\log g = 1.50 \pm 0.25$).

In the best model, the hotspot with 19°.6 angular dimension covers 10.9 per cent of the visible disc outer rim and it is situated at longi-

Table 8. Results of the analysis of HD170582 V-band light curve obtained by solving the inverse problem for the Roche model with an accretion disc around the more-massive (hotter) gainer in critical non-synchronous rotation regime. Symbols are as in Table 6.

Quantity		Quantity	
n	455	$\mathcal{M}_1 [\mathrm{M}_\odot]$	9.0 ± 0.2
$\Sigma(\mathrm{O} - \mathrm{C})^2$	0.1542	$\mathcal{M}_2 [\mathrm{M}_\odot]$	1.9 ± 0.1
σ_{rms}	0.0184	$\mathcal{R}_1 [\mathrm{R}_\odot]$	5.8 ± 0.3
$i[°]$	67.4 ± 0.4	$\mathcal{R}_2 [\mathrm{R}_\odot]$	15.6 ± 0.2
F_d	0.65 ± 0.02	$\log g_1$	3.86 ± 0.1
$T_\mathrm{d}[\mathrm{K}]$	5700 ± 200	$\log g_2$	2.33 ± 0.1
$d_\mathrm{e}[a_\mathrm{orb}]$	0.154 ± 0.004	M_bol^1	-4.0 ± 0.2
$d_\mathrm{c}[a_\mathrm{orb}]$	0.041 ± 0.004	M_bol^2	-2.6 ± 0.1
a_T	7.1 ± 0.3	$a_\mathrm{orb}[\mathrm{R}_\odot]$	61.2 ± 0.2
f_1	22.8 ± 0.6	$\mathcal{R}_\mathrm{d}[\mathrm{R}_\odot]$	20.8 ± 0.3
F_1	1.00	$d_\mathrm{e}[\mathrm{R}_\odot]$	2.5 ± 0.1
$T_1[\mathrm{K}]$	18000	$d_\mathrm{c}[\mathrm{R}_\odot]$	9.5 ± 0.1
$T_2[\mathrm{K}]$	8000		
$A_\mathrm{hs} = T_\mathrm{hs}/T_\mathrm{d}$	1.73 ± 0.1		
$\theta_\mathrm{hs}[°]$	19.0 ± 2.0		
$\lambda_\mathrm{hs}[°]$	332.0 ± 6.0		
$\theta_\mathrm{rad}[°]$	25.0 ± 5.0		
$A_\mathrm{bs} = T_\mathrm{bs}/T_\mathrm{d}$	1.43 ± 0.1		
$\theta_\mathrm{bs}[°]$	56.0 ± 3.0		
$\lambda_\mathrm{bs}[°]$	141.0 ± 5.0		
Ω_1	13.10 ± 0.04		
Ω_2	2.26 ± 0.02		

tude $\lambda_\mathrm{hs} \approx 334°$, roughly between the components of the system, at the place where the gas stream falls on to the disc (Lubow & Shu 1975). The temperature of the hotspot is approximately 66 per cent higher than the disc edge temperature, i.e. $T_\mathrm{hs} \approx 9000$ K.

Although including the hotspot region into the model improves the fit, it cannot explain the light-curve asymmetry completely. By introducing one additional bright spot, larger than the hotspot and located on the disc edge at $\lambda_\mathrm{bs} \approx 135°$, the fit becomes much better, i.e. has a lower χ^2. This bright spot has $T_\mathrm{bs} \approx 7900$ K and with 56°.2 angular dimension covers 31.2 per cent of the visible disc outer rim.

The hot and bright spots might be tentatively identified with shock regions, characterized by higher density and higher temperature than the surrounding medium, revealed in hydrodynamical simulations of mass transfer in close binaries by Bisikalo et al. (1998, 1999, 2003). In particular, the hotspot is near the place where a ballistic trajectory of a particle released in the inner Lagrangian point intersects the accretion disc. The bright spot could correspond to the *hotline*, a shock region that, according to Bisikalo et al. (2003), should appear as product of the interaction of the circumdisc halo and the stream.

It is interesting to determine where the light centres of helium absorption components C1 and C2 calculated in Section 4.3 are located in the system. The C1 light centre is on the disc outer rim in the second quadrant and C2 is roughly in the direction of the hotspot but far from the disc outer rim. Actually, the large $r = 45.9\,\mathrm{R}_\odot$ indicates a position inside the donor for C2. This is inconsistent with the donor temperature which is not enough for forming helium absorption. For the same reason, an origin at the base of the gas stream is also hard to accept. However, we notice that the positions for the components were determined assuming Keplerian orbits (equation 8). Therefore, a possible interpretation for the puzzling result is the existence of vertical motions in the hotspot region, a wind where He I 5875 absorption occurs, characterized by high temper-

ature ($T \geq 10\,000$) and projected velocities larger than Keplerian. This wind is really expected in the stream/disc interaction region according to models of interacting close binaries (van Rensbergen et al. 2008; Deschamps et al. 2013).

We find a gainer mass of 9 M$_\odot$ too high for a temperature of 18 000 K. This B-type dwarf should have a temperature of 21 000 K (Lang 1999). It is possible that the gainer temperature found in the analysis of the SED (Section 6) and used in our model is biased to low temperatures because of the presence of the low-temperature circumprimary disc and the low visibility of the gainer, which is almost completely hidden by the disc. To explore the sensitivity of our solution to the temperature of the gainer, we searched for the best synchronous solution with $T_1 = 21\,000$ K, and we found basically the same parameters that for the cooler gainer case (Table 9). Our conclusion is that the best solution is almost insensitive to the choice of the gainer temperature among reasonable values for early B-type stars, and that the parameters found in our analysis are robust in this sense.

6 SPECTRAL ENERGY DISTRIBUTION, REDDENING AND DISTANCE

We used the Spanish Virtual Observatory SED Analyzer[8] (VOSA; Bayo et al. 2008) to get the broad-band photometric fluxes published for HD 170582 (Table 10). We performed a fit to the SED by means of the Marquant–Levenberg non-linear least-squares algorithm by minimization of χ^2 of the function:

$$f_\lambda = f_{\lambda,0} 10^{-0.4 E(B-V)[k(\lambda-V)+R(V)]}, \qquad (12)$$

where

$$f_{\lambda,0} = (R_2/d)^2 [(R_1/R_2)^2 f_{1,\lambda} + f_{2,\lambda}], \qquad (13)$$

and f_1 and f_2 are the fluxes of the primary and secondary star, $k(\lambda - V) \equiv E(\lambda - V)/E(B - V)$ is the normalized extinction curve, $R(V) \equiv A(\lambda)/E(B - V)$ is the ratio of reddening to extinction at V, d is the distance to the binary and R_1/R_2 is the ratio of the primary radius to the secondary radius. We used the average Galactic Extinction Curve parametrized by Fitzpatrick & Massa (2007, hereafter FM07) to calculate reddened fluxes. The code was implemented in ORIGIN.[9] The stellar fluxes were taken from the grid of ATLAS9 Kurucz ODFNEW /NOVER models available in the Theoretical Spectra Web Server of the Spanish Virtual Observatory.[10] We used fluxes calculated with solar chemical abundance and microturbulence velocity 2 km s^{-1}. The free parameters of the fit were R_2/d and $E(B - V)$. We fixed $R = 3.0$ (FM07), $\log g_1 = 4.0$, $T_2 = 8000$ K, $\log g_2 = 1.5$ and $R_1/R_2 = 0.346$. We tried models with temperatures $T_1 = 15, 18, 20$ and 22 kK. The deviating points from Lahulla & Hilton (1992) at λ 3650 Å, and that of the DENIS survey at λ 7862 Å were not considered in the fit. While the large deviation of the last one suggests an instrumental error, the first one could indicate a diminished Balmer jump regarding a normal star, as seen in some Be stars, a fact that is generally associated with the effect of a circumstellar envelope (Goraya 1986). It is important to keep in mind that the results of this section are limited to the validity of using the average Galactic extinction, which is not always true for different line of sights of our Galaxy (FM07). However, it is the
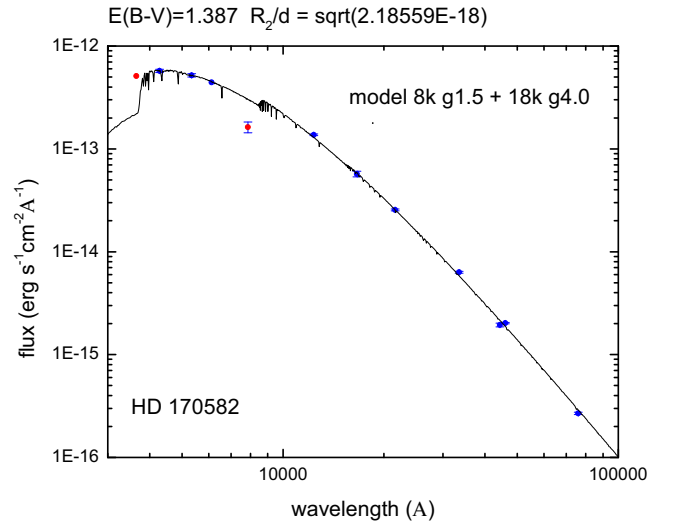
Figure 11. Spectral energy distribution and the best fit given by equation (12), excluding the two outliers discussed in the text.

only approximation possible at this moment. Another limitation of the model is the absence of the circumprimary disc component.

The best fit, minimizing χ^2, gave $T_1 = 18\,000 \pm 1500$ K, $R_2/d = (1.478 \pm 0.045) \times 10^{-9}$ and $E(B - V) = 1.387 \pm 0.015$ (Fig. 11). As noted before T_1 is too low for the gainer mass derived in Section 5.2. This could indicate that we are fitting the flux of the gainer plus the surrounding optically thick accretion disc, a pseudo-photosphere with a stellar-like flux distribution and temperature lower than the gainer. A disc surrounding a hot gainer and mimicking a cooler star is observed in the interacting binaries RX Cassiopeiae, W Crucis and W Serpentis (Plavec 1992); the possible connection of HD 170582 with W Serpentis stars is discussed in Section 7.

The relatively large extinction matches published values of Galactic dust reddening and extinction in the region of HD 170582, viz. $E(B - V) = 1.37 \pm 0.06$ and 1.60 ± 0.07 (NASA/IPAC infrared science archive; based on Schlegel, Finkbeiner & Davis 1998; Schlafly & Finkbeiner 2011). Our colour excess differs from that derived by Lahulla & Hilton (1992), viz. $E(B - V) = 0.17$, but they assumed a luminosity class V and a single A9 star in their analysis.

Although the colour excess is relatively well constrained from the SED analysis, the strength of diffuse interstellar bands (DIBs) indicate a different value. These bands are absorption lines observed in the optical and infrared spectra of reddened stars (Herbig 1995); the strength of some of them roughly correlated with the colour excess produced by interstellar reddening. We measured the EWs of DIBs located at 5780, 5797 and 8620 Å (EW = 0.30 ± 0.01, 0.08 ± 0.01 and 0.20 ± 0.01 Å, respectively) and used the relations given by Munari (2000) and Weselak et al. (2008) to estimate $E(B - V) = 0.55 \pm 0.15$. On the other hand, the strength of K I 7699 suggests $E(B - V) \approx 0.5$ (Munari & Zwitter 1997).

A possible explanation for this discrepancy is the existence of intrinsic reddening produced by circumstellar matter, such as $E(B - V) = E(B - V)_{is} + E(B - V)_{cm}$, where $E(B - V)_{is} = 0.55$ is the interstellar reddening and $E(B - V)_{cm} = 0.82$ is the circumstellar reddening. The existence of anomalous DIBs, weaker than expected for the stellar reddening, has been reported for the Be stars HD 44458 and HD 63462 (Porceddu, Benvenuti & Krelowski 1992) and the Herbig Be star HD 53367 (Whittet & Blades 1980) and attributed to circumstellar matter. The idea behind is that the carriers

Table 9. Results of the analysis of HD170582 *V*-band light curve obtained by solving the inverse problem for the Roche model with an accretion disc around the more-massive (hotter) gainer in synchronous rotation regime. Symbols are as in Table 6 but the gainer temperature is 21 000 K.

Quantity		Quantity	
n	455	$\mathcal{M}_1[\mathrm{M_\odot}]$	9.0 ± 0.2
$\Sigma(\mathrm{O-C})^2$	0.1516	$\mathcal{M}_2[\mathrm{M_\odot}]$	1.9 ± 0.1
σ_{rms}	0.0183	$\mathcal{R}_1[\mathrm{R_\odot}]$	5.5 ± 0.2
$i[°]$	67.4 ± 0.4	$\mathcal{R}_2[\mathrm{R_\odot}]$	15.6 ± 0.2
F_{d}	0.66 ± 0.02	$\log g_1$	3.9 ± 0.1
$T_{\mathrm{d}}[\mathrm{K}]$	5430 ± 200	$\log g_2$	2.33 ± 0.1
$d_{\mathrm{e}}[a_{\mathrm{orb}}]$	0.156 ± 0.004	M_{bol}^1	-4.5 ± 0.2
$d_{\mathrm{c}}[a_{\mathrm{orb}}]$	0.038 ± 0.004	M_{bol}^2	-2.6 ± 0.1
a_{T}	8.5 ± 0.4	$a_{\mathrm{orb}}[\mathrm{R_\odot}]$	61.2 ± 0.2
f_1	1.00	$\mathcal{R}_{\mathrm{d}}[\mathrm{R_\odot}]$	21.2 ± 0.3
F_1	0.187 ± 0.004	$d_{\mathrm{e}}[\mathrm{R_\odot}]$	2.4 ± 0.1
$T_1[\mathrm{K}]$	21000	$d_{\mathrm{c}}[\mathrm{R_\odot}]$	9.6 ± 0.1
$T_2[\mathrm{K}]$	8000		
$A_{\mathrm{hs}} = T_{\mathrm{hs}}/T_{\mathrm{d}}$	1.85 ± 0.1		
$\theta_{\mathrm{hs}}[°]$	19.8 ± 2.0		
$\lambda_{\mathrm{hs}}[°]$	330.6 ± 6.0		
$\theta_{\mathrm{rad}}[°]$	10.0 ± 8.0		
$A_{\mathrm{bs}} = T_{\mathrm{bs}}/T_{\mathrm{d}}$	1.56 ± 0.1		
$\theta_{\mathrm{bs}}[°]$	56.8 ± 3.0		
$\lambda_{\mathrm{bs}}[°]$	103.7 ± 6.0		
Ω_1	11.25 ± 0.04		
Ω_2	2.26 ± 0.02		

of diffuse bands (whatever they are), cannot survive in the relatively dense regions of circumstellar shells (Porceddu et al. 1992). If this were the case for HD 170582, then its relatively large reddening should not be related to the location of the system in the molecular cloud L 379, but to the presence of circumstellar matter. Actually, the location of the system in a dense interstellar environment seems not to be related to their nature of DPV, since many of them exist in not so dense regions.

From $R_2/d = (1.478 \pm 0.045) \times 10^{-9}$ determined from the SED fitting and using $R_2 = 15.6 \pm 0.2$ R$_\odot$ determined from the LC model we obtain a distance of 238 ± 10 pc. This figure compares well with the distance 210 pc derived by Lahulla & Hilton (1992). Results of this section are summarized in Table 11.

7 CONCLUSIONS

We have investigated spectroscopically and photometrically the DPV HD 170582. It turns to be an interacting binary consisting of an 8000 K supergiant of solar abundance transferring matter to an early B-type star. From an RV study based on high-resolution spectra, we find a mass function of $f(M) = 4.81 \pm 0.01$ M$_\odot$. Under the reasonable assumption of a donor with spin-orbit synchronization filling its Roche lobe, we derive a system mass ratio of $q = 0.21$. We model the light curve including synthetic stellar fluxes and an optically thick accretion disc around the B-type star. Using an inverse-problem solving algorithm, we derive the system inclination, stellar masses, radii, temperatures, surface gravities and bolometric luminosities along with the properties of the disc (e.g. the radial and vertical extension and the temperature as a function of the radial coordinate). All these parameters along with the donor rotational velocity, are given in Tables 7–9 and 11.

The disc is luminous, contributing between 30 and 40 per cent to the system luminosity at the *V* band, depending on the orbital

phase. The gainer is almost completely hidden by the disc and its contribution to the total light is only 10 per cent; their temperature results low for the stellar mass probably due to this handicap. However, we show that our system parameters are robust for a range of reasonable gainer temperatures. Our study indicates that for HD 170582, and possibly for others DPVs with luminous discs, the optical and infrared flux is dominated by the donor and the disc, a fact that should be taken into account when fitting the SED in this wavelength range. The best model of the accretion disk includes two relatively hot bright spots in the outer disc rim, in opposite positions, whose properties are given in Tables 7 and 8. One of these spots is located at the region where the gas stream hits the accretion disc and the other could be explained as a shock region as indicated by previous simulations of gas dynamics in close binary systems.

We find that HD 170882 shows spectroscopic properties similar to other DPVs like AU Monocerotis, V 393 Scorpii, DQ Velorum and OGLE 05155332-6925581 (Mennickent et al, 2008, 2012a,b; Barría et al. 2013, 2014; Garrido et al. 2013). These properties include the existence of an optically thick disc surrounding a B-type star and evidence for stream–disc interaction. In this sense, HD 170582 could be related to the strongly interacting binaries of the W Serpentis type (e.g. Plavec & Koch 1978; Plavec 1980, 1992); however, we observe in HD 170582 the distinctive characteristics of DPVs which place them apart from the W Serpentis group, namely the relatively constant orbital period (it is variable in the Serpentids), and the presence of a long photometric periodicity lasting about 33 times the orbital period. To our knowledge, these last two features have never been reported simultaneously in any W Serpentis star. For instance, the eclipsing W Serpentis star RX Cas also shows a primary hidden by an accretion disc (Andersen, Pavlovski & Piirola 1989; Djurašević 1992), and unequal maxima in the orbital light curve (Gaposchkin 1944), but it shows a variable orbital period of 32.327 39 d and $\mathrm{d}P_\mathrm{o}/\mathrm{d}t \sim 10^{-7}$ (Pustylnik, Kalv & Harvig 2007) and a long photometric cycle of 516.06 d (Gaposchkin 1944).

Among the DPVs so far studied, HD 170582 is unique in showing a double He I 5875 line; two absorption lines move in antiphase during the orbital cycle. The light centre of one of these absorptions is located in the disc outer rim in the second quadrant, and the other roughly in the direction of the hotspot, but well far from the disc outer edge and inside the donor. This position is contradictory with formation of helium absorption lines, hence we suggest that significant vertical motions are present near the hotspot producing an RV half-amplitude larger than expected for Keplerian motion. This wind is predicted by models of interacting close binaries and could be a mechanism of mass and angular momentum loss in these systems (van Rensbergen et al. 2008; Deschamps et al. 2013).

From the SED analysis, we find a distance of 238 ± 10 pc and a relatively large colour excess, compatible with reported average measurements in the field. However, DIBs suggests a lower colour excess. This might be explained by the presence of circumstellar matter.

We will investigate in a forthcoming paper the long-term variability, the properties of the circumstellar matter and the evolutionary stage of this system.

Table 10. Summary of broad-band photometric fluxes compiled from literature. Information about the DENIS public survey is found at http://cdsweb.u-strasbg.fr/denis.html.

Filter	$\lambda(\text{Å})$	f_λ (erg s^{-1} cm^{-2} Å^{-1})	ef_λ (erg s^{-1} cm^{-2} Å^{-1})	Reference
Johnson U	3600.00	5.120e−13	−	Lahulla & Hilton 1992
TYCHO/TYCHO.B	4280.00	5.747e−13	2.064e−14	Høg et al. (2000)
TYCHO/TYCHO.V	5340.00	5.198e−13	1.915e−14	Høg et al. (2000)
SLOAN/SDSS.r	6122.33	4.428e−13	−	Adelman-McCarthy et al. (2008)
DENIS/DENIS.I	7862.10	1.631e−13	1.952e−14	DENIS 3rd Release (Sep. 2005)
2MASS/2MASS.J	12 350.00	1.371e−13	2.525e−15	Skrutskie et al. (2006)
2MASS/2MASS.H	16 620.00	5.710e−14	3.524e−15	Skrutskie et al. (2006)
2MASS/2MASS.Ks	21 590.00	2.552e−14	5.642e−16	Skrutskie et al. (2006)
WISE/WISE.$W1$	33 526.00	6.331e−15	1.283e−16	Wright et al. (2010)
Spitzer/IRAC.$I2$	44 365.78	1.942e−15	7.778e−17	Benjamin et al. (2003) and Churchwell et al. (2009)
WISE/WISE.$W2$	46 028.00	2.025e−15	3.358e−17	Wright et al. (2010)
Spitzer/IRAC.$I4$	75 891.59	2.684e−16	6.548e−18	Benjamin et al. (2003) and Churchwell et al. (2009)
WISE/WISE.$W3$	115 608.00	6.002e−17	1.161e−18	Wright et al. (2010)
WISE/WISE.$W4$	220 883.00	7.216e−18	9.638e−19	Wright et al. (2010)

Table 11. Summary of light-curve ephemerides, donor model spectrum and SED fit for HD 170582.

Parameter	Value
Ephemeris$_{\text{max, orbital}}$	$2452118.275 + 16.871 \times E$
Ephemeris$_{\text{max, long}}$	$2452070.9 + 587 \times E$
$E(B − V)$	1.387 ± 0.015
d	238 ± 10 pc
T_1	$18\,000 \pm 1500$ K
T_2	8000 ± 100 K
$v_{2r}\sin i$	44 ± 2 km s^{-1}
ξ	1.0 ± 0.7 km s^{-1}.
$\log g_2$	1.7 ± 0.5

REFERENCES

Adelman-McCarthy J. K. et al., 2008, ApJS, 175, 297
Andersen J., Pavlovski K., Piirola V., 1989, A&A, 215, 272
Asplund M., Grevesse N., Sauval A. J., Scott P., 2009, ARA&A, 47, 481
Barría D., Mennickent R. E., Schmidtobreick L., Djurašević G., Kołaczkowski Z., Michalska G., Vučković M., Niemczura E., 2013, A&A, 552, A63
Barría D., Mennickent R. E., Graczyk D., Kołaczkowski Z., 2014, A&A, 567, A140
Bayo A., Rodrigo C., Barrado Y Navascués D., Solano E., Gutiérrez R., Morales-Calderón M., Allard F., 2008, A&A, 492, 277
Benjamin R. A. et al., 2003, PASP, 115, 953
Bevington P. R., Robinson D. K., 1992, Data Reduction and Error Analysis for the Physical Sciences, 2nd edn. McGraw-Hill, New York

Bisikalo D. V., Boyarchuk A. A., Chechetkin V. M., Kuznetsov O. A., Molteni D., 1998, MNRAS, 300, 39
Bisikalo D. V., Boyarchuk A. A., Chechetkin V. M., Kuznetsov O. A., Molteni D., 1999, Astron. Rep., 43, 797
Bisikalo D. V., Boyarchuk A. A., Kaigorodov P. V., Kuznetsov O. A., 2003, Astron. Rep., 47, 809
Castelli F., Hubrig S., 2004, A&A, 425, 263
Charbonneau P., 1995, ApJS, 101, 309
Churchwell E. et al., 2009, PASP, 121, 213
de Mink S. E., Pols O. R., Glebbeek E., 2007, in Stancliffe R. J., Houdek G., Martin R. G., Tout C. A., eds, AIP Conf. Proc. Vol. 948, UNSOLVED PROBLEMS IN STELLAR PHYSICS: A Conference in Honor of Douglas Gough. Am. Inst. Phys., New York, p. 321
Dennis J. E., Torczon V., 1991, SIAM J. Optim., 1, 448
Deschamps R., Siess L., Davis P. J., Jorissen A., 2013, A&A, 557, A40
Djurašević G., 1992, Ap&SS, 197, 17
Djurašević G., Latković O., Vince I., Cséki A., 2010, MNRAS, 409, 329
Eggleton P., 2006, Evolutionary Process in Binary and Multiple Stars. Cambridge Univ. Press, Cambridge
Fitzpatrick E. L., Massa D., 2007, ApJ, 663, 320 (FM07)
Gaposchkin S., 1944, ApJ, 100, 230
Garrido H. E., Mennickent R. E., Djurašević G., Kołaczkowski Z., Niemczura E., Mennekens N., 2013, MNRAS, 428, 1594
Goraya P. S., 1986, MNRAS, 222, 121
Gray D. F., 2005, The Observation and Analysis of Stellar Photospheres, 3rd edn. Cambridge Univ. Press, Cambridge
Herbig G. H., 1995, ARA&A, 33, 19
Hilditch R. W., 2001, An Introduction to Close Binary Stars. Cambridge Univ. Press, Cambridge
Høg E. et al., 2000, A&A, 355, L27
Houk N., Smith-Moore M., 1988, Michigan Catalogue of Two-dimensional Spectral Types for the HD Stars. Volume 4, Declinations -26.0 to -12.0. Univ. Michigan, Ann Arbor, MI
Kolbas V., Dervişoğlu A., Pavlovski K., Southworth J., 2014, MNRAS, 444, 3118
Kurucz R., 1993, CD-ROM 18: SYNTHE Spectrum Synthesis Programs and Line Data
Lahulla J. F., Hilton J., 1992, A&AS, 94, 265
Lang K. R., 1999, Astrophysical Formulae. Springer, New York
Lubow S. H., Shu F. H., 1975, ApJ, 198, 383
Lucy L. B., 2005, A&A, 439, 663
Mennickent R. E., 2013, Cent. Eur. Astrophys. Bull., 37, 41
Mennickent R. E., Rosales J., 2014, Inf. Bull. Var. Stars, 6116, 1
Mennickent R. E., Pietrzyński G., Diaz M., Gieren W., 2003, A&A, 399, L47
Mennickent R. E., Kołaczkowski Z., Michalska G., Pietrzyński G., Gallardo R., Cidale L., Granada A., Gieren W., 2008, MNRAS, 389, 1605

Mennickent R. E., Djurašević G., Kołaczkowski Z., Michalska G., 2012a, MNRAS, 421, 862

Mennickent R. E., Kołaczkowski Z., Djurašević G., Niemczura E., Diaz M., Curé M., Araya I., Peters G. J., 2012b, MNRAS, 427, 607

Munari U., 2000, in Porceddu I., Aiello S., eds, Italian Physical Society Conf. Proc. Vol. 67, Molecules in Space and in the Laboratory. Italian Physical Society, Bologna, p. 179

Munari U., Zwitter T., 1997, A&A, 318, 269

Niemczura E., Połubek G., 2006, in Fletcher K., ed., ESA SP-624: SOHO 18/GONG 2006/HELAS I Beyond the Spherical Sun. ESA, Noordwijk, p. 92

Packet W., 1981, A&A, 102, 17

Petrovic J., Langer N., van der Hucht K. A., 2005, A&A, 435, 1013

Plavec M. J., 1980, in Plavec M.J., Popper D.M., Ulrich R.K., eds, Proc. IAU Symp. 88, Close binary stars: Observations and Interpretation. Reidel, Dordrecht, p. 251

Plavec M. J., 1992, in Drissen L., Leitherer C., Nota A., eds, ASP Conf. Ser. Vol. 22, Nonisotropic and Variable Outflows from Stars. Astron. Soc. Pac., San Francisco, p. 47

Plavec M., Koch R. H., 1978, Inf. Bull. Var. Stars, 1482, 1

Pojmański G., 1997, Acta Astron., 47, 467

Poleski R., Soszyński I., Udalski A., Szymański M. K., Kubiak M., Pietrzyński G., Wyrzykowski Ł., Ulaczyk K., 2010, Acta Astron., 60, 179

Popham R., Narayan R., 1991, ApJ, 370, 604

Porceddu I., Benvenuti P., Krelowski J., 1992, A&A, 257, 745

Press W. H., Teukolsky S. A., Vetterling W. T., Flannery B. P., 1992, Numerical Recipes in Fortran. The Art of Scientific Computing, Vol. 120. Cambridge Univ. Press, Cambridge

Przybilla N., Butler K., Becker S. R., Kudritzki R. P., 2006, A&A, 445, 1099

Pustylnik I., Kalv P., Harvig V., 2007, Astron. Astrophys. Trans., 26, 31

Rafert J. B., Twigg L. W., 1980, MNRAS, 193, 79

Sbordone L., 2005, Mem. Soc. Astron. Ital., 8, 61

Schlafly E. F., Finkbeiner D. P., 2011, ApJ, 737, 103

Schlegel D. J., Finkbeiner D. P., Davis M., 1998, ApJ, 500, 525

Skrutskie M. F. et al., 2006, AJ, 131, 1163

Stellingwerf R. F., 1978, ApJ, 224, 953

van Rensbergen W., De Greve J. P., De Loore C., Mennekens N., 2008, A&A, 487, 1129

von Zeipel H., 1924, MNRAS, 84, 702

Weselak T., Galazutdinov G. A., Musaev F. A., Krełowski J., 2008, A&A, 484, 381

Whittet D. C. B., Blades J. C., 1980, MNRAS, 190, 41p

Wright E. L. et al., 2010, AJ, 140, 1868

Zahn J.-P., 1975, A&A, 41, 329

Zahn J.-P., 1977, A&A, 57, 383

This paper has been typeset from a TEX/LATEX file prepared by the author.